Advecting heating by hot fluids of an Alpine fissure in Lauzière Granite (Belledonne massif, Western Alps)

5   Emilie Janots[1,2], Alexis Grand'Homme[1], Matthias Bernet[1], Damien Guillaume[3], Edwin Gnos[4], Marie-Christine Boiron[5], Magali Rossi[6], Anne-Magali Seydoux-Guillaume[3], Roger De Ascenção Guedes[7]

[1] Univ. Grenoble Alpes, CNRS, IRD, IFSTTAR, ISTerre, 38000 Grenoble, France
10   [2] Department of Earth and Environmental Sciences, Ludwig-Maximilians-Universität Munich, Luisenstr, 37, 80333 Munich, Germany
[3] Univ Lyon, UJM-Saint-Etienne, UCA, CNRS, IRD, LMV UMR 6524, F-42023, SAINT-ETIENNE, France.
[4] Natural History Museum of Geneva, 1 route de Malagnou, CH-1208 Geneva
[5] Université de Lorraine, CNRS, GeoRessources, F- 54000 Nancy, France
[6] Univ. Grenoble Alpes, Univ. Savoie Mont-Blanc, CNRS, EDYTEM, 73 000 Chambéry
15   [7] Editions du Piat, Glavenas, F-43200 Saint-Julien-du-Pinet, France

Correspondence to: Emilie Janots (emilie.janots@univ-grenoble-alpes.fr)

Abstract. A multi-method approach investigation in the Lauzière granite, located in the external Belledonne massif of the French Alps, reveals unusually hot hydrothermal conditions in vertical open fractures (Alpine-type clefts), caused by
20   advective heating. The host-rock granite shows sub-vertical mylonitic microstructures and partial retrogression at temperatures of <400°C during Alpine tectonometamorphism. Novel zircon fission-track (ZFT) data in the granite give ages at 16.3 ± 1.9 and 14.3 ± 1.6 Ma, confirming that Alpine metamorphism was high enough to reset the pre-alpine cooling ages and that the Lauzière granite had already cooled below <240-280°C and was exhumed to <10 km at that time. Novel microthermometric data and chemical compositions of fluid inclusions obtained on millimetric monazite and on quartz
25   crystals from the same cleft indicate early precipitation of monazite from a hot fluid at T>410°C, followed by a main stage of quartz growth at 300-320°C and 1.5-2.2 kbar. Previous Th-Pb dating of cleft monazite at 12.4 ± 0.1 Ma clearly indicates that this hot fluid infiltration took place significantly later than the peak of the Alpine metamorphism. Advective heating due to the hot fluid caused rejuvenation of the ZFT age at 10.3 ± 1.0 Ma in the cleft hanging wall. The results attest of highly dynamic fluid pathways, allowing the circulation of deep mid-crustal fluids, 150-250°C hotter than the host-rock, affecting
30   the thermal regime at the wall-rock of the Alpine-type cleft for a duration of 1-3 My. Such advecting heating may represent a pitfall source for exhumation reconstructions.

1 Introduction

Geochronological datasets in external parts of mountain belts are primordial to date metamorphism, deformation and fluid activity, to model exhumation rates, and to appreciate the role of tectonic activity, topography and climate influence on orogenic evolution. Geochronological data can either be interpreted as apparent cooling ages or crystallisation ages.

5 Apparent cooling ages are assumed to record the time at which a rock cooled below the closure temperature of the thermochronometer. Exhumation rates can thus be derived by correlating the apparent cooling ages with the closure depth for a given geothermal gradient (Brandon et al., 1998; Willet and Brandon, 2013). For geochronometers with closure temperatures above the rock/mineral (re)-crystallization temperature, geochronological data record the age of crystallisation. Petrochronology is an emerging field of Earth Sciences aiming to characterize the crystallisation conditions associated with

10 age based on petrological characterisations (Engi et al., 2017). Combining thermochonological data with crystallisation ages is powerful to evaluate the possibility of increased tectonic or fluid activity, which can efficiently affect exhumation rates. Crystallisation during exhumation (retrogression) is commonly related to deformation and fluid circulation, because retrogression involves hydration reactions and mass transfer requires fluid (e.g., Austrheim and Griffin, 1985; Putnis and Austrheim, 2010). This is particularly true for basement rocks in external parts of orogenic belts, where crystalline rocks

15 mainly made of anhydrous minerals are submitted to low-temperature retrogression, which are slowing down mineral reaction kinetics. For example in the external crystalline massifs (ECM) of the Alps, retrogression occurs at temperatures <400°C and is commonly localized in highly deformed domains (e.g. shear zone, mylonite; Bellanger et al., 2015; Rossi et al., 2005) with evidence of fluid circulation causing vein formation, metasomatism, or fluid assisted reactions (Rossi and Rolland, 2014). Ascending fluids can also modify the temperature gradient by advective heating, but the influence of fluid

20 flow on thermochronological data is seldom considered in exhumation reconstructions (Derry et al., 2009; Whipp and Ehlers, 2007), and remains to be quantified through numerical modelling. In natural environments, the impact of hydrothermal activity on the thermal structure is difficult to quantify because it requires evaluating the fluid flux in a system that is partially open and multistage. New insights have recently been gained from in-situ monazite-(Ce) (hereafter called monazite) dating in hydrothermal clefts (open fissures partly filled by hydrothermally grown minerals), providing precise

25 constraints on the timing, duration and periodicity of hydrothermal precipitations during late-stage deformation (Bergemann et al., 2017; Berger et al., 2013; Janots et al., 2012). Especially, the general overlap of initial crystallization age of cleft monazite with zircon fission-track (ZFT) data (Berger et al., 2013; Gnos et al., 2015; Grand'Homme et al., 2016), and possible feedback between fluid flow, monazite precipitation, and thermochronometer-derived exhumation rates remain to be understood (Grand'Homme et al., 2016). On one hand, this similarity may indicate that monazite crystallized when the

30 fluid cooled down under a temperature close to that recorded by ZFT (Gnos et al., 2015). On the other hand, this is contradictory with the short-duration and episodic growth of cleft monazite (Janots et al., 2012) suggesting that it precipitates due to tectonic/hydrothermal activity rather than by progressive cooling during exhumation (Bergmann et al., 2017; Gasquet et al., 2010; Grand'Homme et al., 2016).

In this paper, LA-ICP-MS and microthermometric data on fluid inclusions were successfully combined with geochronological data on monazite crystals to reveal local advective heating due to hydrothermal circulation in vein systems during exhumation of the Lauzière Granite (Belledonne massif, Western Alps). The impact of advective heating on the thermal regime of the host-rock was then evaluated from ZFT data in host rock granite samples collected at the direct contact, 30 meters and 100 meters away from the cleft.

2 Geological Settings and samples

The Alpine belt results from the closure of the Tethys Ocean and the subsequent collision between the Eurasian and Adriatic plates. The investigated outcrop is located in the Lauzière granite (Fig. 1), in the northern prolongation of the Belledonne massif, which belongs to the external crystalline massifs (ECM; Fig. 1a). The ECM consist of blocks of Variscan European basement thrusted under the internal domains, following the activation of the Penninic front during Oligocene-Miocene times (Dumont et al., 2008). Related metamorphism was never evaluated in the Lauzière granite, and remains poorly constrained in the Belledonne massif (320°C-350°C; Nziengui, 1993). It is assumed to lie between the values of the Mont Blanc massif in the north (400°C, <5 kbar; Rolland et al., 2003; Rossi et al., 2005) and the Oisans massif to the south (270-360°C, 2-5 kbar; review in Bellanger et al., 2015). A complex geochronological dataset exists for the metamorphism recorded in shear zones and veins in the ECM, with three age-groups at ca. 24-30 Ma; 20-12 Ma and 12-6 Ma, attributed to the different deformation stages (Gasquet et al., 2010; Leloup et al., 2005; Rolland and Rossi, 2016). Underthrusting of the ECM is generally estimated to have occurred around 30 Ma (Bellanger et al., 2015; Cenki-Tok et al., 2011; Nziengui, 1993; Rolland and Rossi, 2016). The Ar–Ar and ZFT datasets suggest that cooling and exhumation started at ca. 18 Ma (Boutoux et al., 2016; Seward and Mancktelow, 1994), in a compressive tectonic regime until 12 Ma (dating in horizontal veins; Bergemann et al., 2017; Gasquet et al., 2010; Rossi and Rolland, 2014). Finally, a transpressive regime (dextral strike slip) prevailed at 12-10 and 6-8 Ma. This has been constrained through in-situ U-Th-Pb dating of monazite crystals collected in vertical fissures (Bergemann et al., 2017; Gasquet et al., 2010; Grand'Homme et al., 2016).

Samples of the Lauzière granite were collected below the "Entre deux roches" pass (Fig. 2a), which is located at the eastern margin of the Lauzière massif, 2 km westward from the major Ornon-Roselend fault separating the ECM from Mesozoic formations and close from tectonic accident to the south (Fig. 1b). In this eastern margin, the deformation is pervasive (mylonite) with N020-040 oriented subvertical foliation. The Lauzière granite is a late-Variscan complex dated at 341 ± 13 Ma (Debon et al., 1998). Despite of variable strain and retrogression, the original K-feldspar-albite-quartz-biotite assemblage of the monzogranite is readily identified microscopically by ubiquitous mm-sized titanite pseudomorphoses (leucoxene). Retrogression is characterized by biotite and K-feldspar breakdown and growth of fine-grained albite and low-temperature white mica. In this outcrop, efficient fluid circulation with relatively high fluid/rock ratio is evidenced by the pervasive retrogression in white mica similar to that described by Rolland and Rossi (2016) in the Mont Blanc massif, and by the presence of subvertical veins that are typically cm-sized. In the case of the investigated Alpine-cleft, a vertical open-

cavity partly filled by hydrothermally grown mineral, the dimensions are however plurimetric in height and length. This cleft is oriented perpendicular to the main host-rock foliation (Fig. 2b). It is filled by mm- to cm-sized quartz (Fig. 2c), albite, adularia, chlorite and also accessory minerals such as anatase, rutile, ilmenite, apatite, monazite, xenotime, and rare sulfosalts as meneghinite (Moëlo et al., 2002). At the cleft contact, the host-rock shows high retrogression with abundant

5 white mica (biotite-free). The cleft contains abundant millimetric monazite grains (prisms up to 9 mm), which were previously dated in-situ using LA-ICP-MS (Grand'Homme et al., 2016). Although the monazite grains were zoned, Th-Pb ages (12.4 ± 0.1 Ma; MSWD = 1.7) and U-Pb ages (12.2 ± 0.2 Ma; MSWD = 1.1) are concordant, with overlap of ages obtained on different grains and in different compositional domains within a grain. This U-Th-Pb dating indicates a short-duration growth of hydrothermal monazite. Furthermore, these monazite crystals contain fluid inclusions, offering the

10 possibility to correlate crystallization age with the physicochemical conditions of the hydrothermal episode. Amongst the 15 hand-specimen containing mm-sized monazite, we separated associations of contiguous monazite and quartz crystals (samples E2R2, E2R3, E2R4) and adjacent quartz crystals (samples E2R1, E2R31). Most quartz crystals are mm-sized, but the E2R3 (-a, -b, -c) and E2R31 (-a, -b) are fragments from centimer-sized crystals. When monazite and quartz were found contiguous, quartz seems to lie over monazite and thus to have grown after it.

15 Quartz and monazite individual crystals were double-polished, and ~200 to 300-µm-thick sections were prepared for fluid inclusion studies (Figs. 3a and 3b).

In addition to the cleft hydrothermal samples, five granitic samples were also collected along a ~100 m profile with no significant elevation difference. Amongst the five host-rock samples prepared for zircon fission track analyses, only 3 provided successful results. Sample collection strategy was aimed to compare the ZFT age obtained at the cleft contact

20 (sample R1) to ages of host-rock samples that remained unaffected by significant late-stage fluid (samples R2 and R3 at 30 m and 100 m of the cleft, respectively). The host-rock samples were taken in area devoid of veins in their direct vicinity. At the cleft contact, the granite show smaller grain size (higher strain) and higher abundance of white mica (higher retrogression) compared to host-rock samples take at different distances of the cleft.

3 Methods

25 ### 3.1 Fluid inclusions analysis

Microthermometric measurements were performed with a Linkam THMS600 heating freezing stage mounted on a BX-51 Olympus microscope at the Geosciences Environnement Toulouse (GET) laboratory and the GeoRessources laboratory (Nancy). Temperatures of the following phase changes were measured: eutectic melting (T_e), ice melting (T_m ice), and total homogenization (T_h). According to the calibration curves and the type of phase changes, temperatures are given with an

30 accuracy of about $\pm 5°C$ for T_e, and $\pm 0.2°C$ for T_m ice and T_h. Fluid composition analyses of inclusions in quartz were carried out by LA-ICP-MS at the GeoRessources laboratory (Nancy, France) following protocols published in Leisen et al. (2012). The LA-ICP-MS system is composed of a GeoLas excimer laser (ArF, 193nm, Microlas, Göttingen, Germany), with

a microscope for sample observation and laser beam focus onto the sample and an Agilent 7500c quadrupole ICP-MS. The sample is located inside a cylindrical ablation cell, attached to a motorized X-Y stage of an optical microscope (® Olympus BX-41). The laser beam is focused onto the sample with a Schwartzschild reflective objective (magnification X 25). The ablated material is carried in helium gas, which is mixed with argon via a cyclone mixer prior to entering the ICP torch,

5   following the procedures outlined by Roedder (1984) and Sheperd et al. (1985).

3.2 Zircon fission tracks

In sample R1 (cleft contact), the smaller grain size (higher strain) resulted in a low zircon yield. Because many zircons were fractured, had strong uranium zoning and/or inclusions, only 7 zircons could be extracted from sample R1, compared to up to 12 zircons in the other samples (R2 and R3). Zircon grains were mounted in Teflon® sheets, polished and etched at 228°C

10   for 16-40 hours in a NaOH-KOH melt. Using the external detector method, all samples were irradiated together with IRMM541 dosimeter glasses and Fish Canyon Tuff age standards at the FRM II reactor in Garching, Germany. External detectors were etched for 18 min in 48% HF at 20°C. Fission-track were counted at the ISTerre Thermochronology laboratory with an Olympus BX2 microscope at 1250x magnification using the FTstage 4.04 system.

4 Results

15   **4.1 Fluid inclusions**

In cleft monazite, primary inclusions occur isolated or form trails of 2-3 inclusions and secondary inclusions are located in healed fracture planes (Figs. 3c and 3d). The size of fluid inclusions ranges from 10x10 µm to less than 4x4 µm for secondary inclusions. In quartz crystals, primary inclusions are also isolated or along trails of 4-5 inclusions parallel to quartz growth faces, whereas secondary inclusions are located on former fissures which crosscut the crystals from rim to

20   core (Figs. 3e and 3f). Quartz populations show euhedral shape with no evidence of deformation microstructure (Diamond and Tarentola; 2015). The size of primary fluid inclusions in quartz is mostly comparable to that of monazite (~10x10 µm) but can reach ~20x30 µm. Secondary fluid inclusions are smaller than 5x5 µm. All the fluid inclusions investigated are bi-phased, liquid and vapour (L-V type), and homogenize to liquid by heating. No solid phase was observed in the studied fluid inclusions.

25   Based on the fluid inclusions petrography and microthermometric results, five different sets of fluid inclusions populations were distinguished in monazite and quartz (Fig. 4; Table 1). In cleft monazite (3 crystals), primary fluid inclusions (MnzP) have T_h ranging from 283.2 to 345.3°C (N = 10). Three secondary inclusions in monazite crystals (MnzS) were large enough for microthermometric measurements, which give T_h between 203.8 to 241.6°C (N = 3). In cleft quartz (5 crystals), two populations of primary inclusions with different T_h were found: the first (QzP1) corresponds to few inclusions

30   with higher T_h (278.3 to 314.9°C; N = 4) compared to the main second group (QzP2; 178.3 to 223.3°C, with a mode around 210°C; N = 46). These two populations are morphologically similar. Secondary inclusions located in quartz samples (QzS)

give lower T_h (120.6 to 147.7°C; N = 8). Eutectic temperature were determined between -21.2 and -23°C, which is in good agreement with T_e for H_2O-NaCl and H_2O-NaCl-KCl systems, respectively at -21.2 and -22.9°C (Bodnar, 2003; Hall et al., 1988). For the entire dataset, T_m ice obtained in quartz and monazite crystals overlap within uncertainty: they range from -6.0 to -9.6°C (Fig. 4), which converts to salinities between 9.2 and 13.5 wt.%NaCl equivalent. There is no significant difference

5 in salinities between the 5 fluid inclusion populations, although fluid inclusions trapped at lower temperature have generally lower salinities. Based on similar T_m ice and T_h values (Fig. 4), the first population of quartz inclusion (QzP1) is considered equivalent to primary inclusions in monazite (MnzP), whereas the secondary fluid inclusion population in monazite (MnzS) overlap with the main group of primary inclusions in quartz (QzP2). Isochores were calculated using equations of Zhang and Frantz (1987) assuming negligible CO_2 (Poty et al., 1974). MnzP and QzP1 fluid inclusions populations give P-T

10 relationships at 11.0 and 11.8 bar/°C, MnzS and QzP2 populations give 16.3 and 17.0 bar/°C and QzS give 21.4 bar/°C (Fig. 6).

In addition to microthermometric data, fluid composition was measured in primary quartz inclusion (Table 2) to evaluate the trace element concentrations and use the Na/K and Na/Li geothermometers (Can, 2002). Amongst the 47 fluid inclusions analysed in quartz, compositions could be retrieved only for 14 of them, due to low intensity signal and the

15 presence of mineral inclusions. Fluid inclusion compositions were successfully obtained only in the fragments of cm-sized quartz (E2R3a, E2R31a and E2R31b). In these quartz fragments, only fluid inclusions with T_h of the QzP2 group were detected and thus fluid inclusion compositions are attributed to this population (Table 1). In the fluid inclusions, only Na, K, Li, and Sr concentrations are systematically above the detection limit of the LA-ICP-MS measurements. The rare earth elements (Y, La, Ce, Pr, Nd, Sm), Th, U, As and Ca are generally below the detection limits. Although fluid inclusions show

20 different cationic contents, the Na/K ratio in the fluid is equivalent for all the studied crystals (3.7 ± 0.3), confirming that equilibrium between feldspar and fluid is achieved. This Na/K ratio corresponds to T of 280-330°C with most values comprised between 300-320°C (Table 2). Similar temperature interval can be obtained based on the Na/K and Na/Li ratio (Fig. 5), using the geothermomether of Verma and Santoyo (1997). Intersection of this T interval with the QzP2 isochore yields a trapping pressure at 1.5-2.2 kbar (Fig. 6).

25 **4.2 Zircon Fission Tracks**

The *R1* sample gave a ZFT central age of 10.3 ± 1 Ma (Fig. 7a), with an age range between 7.2 and 16.7 Ma. The *R2* sample gave a ZFT central age of 16.3 ± 1.9 Ma (Fig. 7b), for an age range between 10.2 and 50.4 Ma. The *R3* sample gave a ZFT central age of 14.3 ± 1.6 Ma (Fig. 7c), with individual grain ages between 5.2 and 20.1 Ma. All samples show relatively high dispersion in the grain age distributions and low $\chi2$ values. Unfortunately, no significant number of horizontal track lengths

30 could be measured to determine the degree of partial annealing in all three samples. Nonetheless, the fissions track in sample R1 appeared shorter than in the other two samples.

5 Discussion

5.1 Hydrothermal activity in the Lauzière Alpine-cleft

Alpine-clefts correspond to fissures that opened up under deformation related to exhumation of the ECM. In Alpine-type clefts, hydrothermal minerals generally precipitate under retrograde metamorphic conditions at temperatures and pressures in

5 the range 150-450°C and 1.4-3.0 kbar, respectively (Fabre et al., 2002; Mullis et al., 1994; Poty et al., 1974). Cleft mineralogy and geochemistry attest of equilibrium with the neighbouring host-rocks (e.g., Sharp et al., 2005). Furthermore, fluid inclusions (e.g., Mullis et al., 1994) and mineral dating (e.g., Janots et al., 2012) indicate episodic crystallisation pulses rather than continuous precipitation due to progressive cooling. Homogenization temperatures and petrologogical observations (primary/secondary) of the fluid inclusions indicate three main stages of fluid inclusions entrapment (Fig. 4):

10   (i)   MnzP + QzP1 with highest homogenization temperatures (278-345°C)

      (ii)   QzP2 + MnzS with intermediate homogenization temperatures (178-242°C)

      (iii) QzS with the lowest homogenization temperatures (121-148°C)

All fluid inclusions have equivalent T_m ice (equivalent salinities) suggesting equilibrium between the fluid and the host-rock. Equilibrium is also supported by the consistency of the Na/K ratio measured in the quartz fluid inclusions (QzP2).

15   Opposite to paragenetic observations that generally suggest a late monazite crystallisation (e.g., Gnos et al., 2015), the petrological observation of quartz lying on monazite and primary fluid inclusions in monazite (MnzP, N = 10; Fig. 4), indicate that monazite precipitates in an early hydrothermal growth stage in the Alpine cleft studied here. This first precipitation stage is independently confirmed by few primary fluid inclusions in quartz (QzP1; N = 4).

    The main episode of quartz growth (QzP2; N = 46) is recorded by secondary fluid inclusions in monazite (MnzS; N

20 = 3; Fig. 4), indicating that monazite growth had ceased by then (Fig. 8). This second episode of hydrothermal growth may be caused by oversaturation reached due to cooling, pressure changes, fluid mixing or deformation (e.g. discussion and references in Bergemann et al., 2017). Geothermometry based on the Na/K ratio (and Na/Li) in quartz fluid inclusions (QzP2) indicate for a main quartz growth at around 300-320°C (Fig. 5) at P = 1.5-2.2 kbar (Fig. 6). The pressure interval of 1.5-2.2 kbar determined from this group is coherent with previous micrometric studies on fluid inclusions in the ECM (Fabre

25 et al., 2002; Mullis et al., 1994; Poty et al., 1974), and the depth expected from previous thermochronological studies in Belledonne and surrounding massifs at that period (Fügenschuh and Schmid, 2003; Glotzbach et al., 2011; Seward and Mancktelow, 1994).

    Alpine-cleft monazite precipitation temperature can be evaluated from the pressure determined for the main phase of quartz growth (QzP2) assuming no major exhumation in the relatively short duration episode (1-3 My, see hereafter)

30 between the main phases of monazite (MnzP) and quartz growth (QzP2). Using the pressure interval of 1.5-2.2 kbar determined with QzP2, intersection with the MnzP isochores indicates a maximal T interval of 410-520°C for monazite growth (Fig. 6). This is one of the rare cases where fluid inclusions document significantly higher fluid temperature compared to the metamorphic host-rock temperatures (Mullis et al., 1994; Boutoux et al., 2014). This hot fluid circulation

would have been overlooked based on quartz fluid inclusions, the number of QzP1 being unrepresentative compared to the QzP2 trapped during the main phase of quartz growth (Fig. 4). To our knowledge, this is one of the first time that fluid inclusions are measured in monazite and it opens a possible avenue to determine early (hot?) stages of hydrothermal precipitation in Alpine cleft. Early precipitation of monazite compared to quartz, may be attributed to its low solubility, but

5   this has to be confirmed in other clefts or for other low-solubility accessory minerals.

5.2 Impact of advective heating on zircon fission track age resetting

Novel ZFT obtained in the Lauzière massif (samples R2 and R3) confirm that metamorphic temperatures were high enough to anneal the pre-Alpine ZFT signature (Yamada et al., 1995). The ZFT dataset indicate that the Lauzière granite cooled down below 240-280°C at around 14-16 Ma (Figs. 7 and 8), in good agreement with previous ZFT data in the in the

10   Belledonne massif (8-15 Ma; Fügenschuh and Schmid, 2003; Seward and Mancktelow, 1994; Figg. 1b). In the cleft hanging-wall, the rejuvenation of the ZFT age at 10.3 ± 1.0 Ma indicates a resetting of the ZFT geochronological system by advective heating due to the hot hydrothermal fluid penetrating the cleft.

It is difficult to quantify the spatial impact of advective heating linked to fluid circulation at the outcrop scale. In the present study, the two samples taken at quite some distance from the cleft (30 m and 100 m) have ZFT ages older than

15   monazite growth in cleft, indicating no significant resetting by related cleft fluid circulation. However, along the eastern margin of the Lauzière granite, fluid circulation is not restricted to clefts but is evidenced in outcrop by retrogression and growth of mica-like phyllosilicates, as evidenced in the Mont Blanc massif by Rolland and Rossi (2016), and the formation of centimetric scale veins. It is thus not possible to rule out that the ZFT dataset of the deformed Lauzière granite was not affected by fluid circulation during the deformation phase responsible of the cleft formation or even during an earlier, ductile

20   deformation stage.

5.3 Geodynamic evolution and fluid circulations during exhumation of the ECM

The ECM are constituted by relatively anhydrous and low-permeability rocks underthrusted at mid-crustal levels during the Oligo-Miocene and then exhumed to form today some of the highest Alpine relief (>4000 m-high peaks). In the Lauzière granite, metamorphic peak, which is not well constrained but estimated <400°C, is assumed to take place at around 24-26

25   Ma (Nziengui, 1993) and more generally at around 24-30 Ma in the ECM. Exhumation in the ECM is normally assumed to start around 18 Ma. Indeed, the new ZFT ages indicate that the Lauzière granite had cooled below 240-280°C and was exhumed at crustal depth of <10 km at 14-16 Ma (Fig. 8). In the Alpine cleft, the well-resolved Th-Pb monazite age of 12.4 ± 0.1 Ma (N = 86) indicates for a short-duration growth of the millimetric monazite crystals (Grand'Homme et al., 2016). Combined with the new microthermometric data, the monazite age is interpreted to date the first stage of hydrothermal

30   growth following the fracturation and infiltration of a hot fluid at T of 410-520°C into the host-rock that had already cooled below 240-280°C (Fig. 8). In other words, there is a 150-250°C temperature difference between the fluid from which monazite precipitates and the fracturing host-rock, in which fluid infiltrates. Assuming an undisturbed crustal geothermal

gradient, it implies that the source of the fluid was at least 6-10 km deeper than the host-rock. Based on the structural data of the subvertical cleft (Fig. 2), this age records the circulation of hot fluids through fractures created during a regional phase of dextral transpressive regime in the ECM (Bergemann et al., 2017; Gasquet et al., 2010). Within the Alpine cleft, quartz growth occurred during a second hydrothermal growth stage at T = 300-320°C, comprised between the monazite growth at

5   12.4 ± 0.1 Ma and the cooling of the cleft hanging wall (sample R3) below 240-280°C, at 10.3 ± 1 Ma (Fig. 8). The difference between these two ages constrains the time range between the infiltration of the hot fluid and cooling down of the cleft wall to temperatures similar to the host-rock, i.e. it fixes the duration interval of the advective heating at around 1-3 My (Fig. 8).

Although the difference between fluid and metamorphic host-rock temperatures (150-250°C) appears unusually
10   high compared to thermal fluid regime previously documented by fluid inclusion in Alpine-type clefts (Mullis et al., 1994; Poty et al., 1974), deep fluid circulation has been already proposed for some other Alpine-type clefts/veins using isotopic and trace element data (Rossi and Rolland, 2014). This thermal difference attests a fluid channelization along pathways of high permeability for upward flow of deep mid-crustal fluids towards the surface. In the ECM, escape of fluids could be originated from topography-driven fluid flow or underthrusted rock dehydration (Hofmann et al., 2004). Fluid channelization
15   required here is expected along steeply oriented deformation structures like shear zones, faults and fractures (e.g., Boutoux et al., 2014; Goncalves et al., 2012; Marquer and Burkhard, 1992; Oliot et al., 2014). Considering the position of the Lauzière granite, possible migrating fluid pathways through deeper crustal levels could localize along the contact between gneiss and metasediments (Ornon-Roselend), or other tectonic accidents located at its southern margin (Fig. 1b). Further relationships between seismicity, fluid circulation and metamorphism could also be considered (Putnis et al., 2017).

20   **6 Conclusion**

This study reveals the potential of investigating fluid inclusions in Alpine-type cleft accessory minerals used more commonly for U-Th-Pb geochronology. Novel fluid inclusion analyses in monazite provide evidence for unusually hot hydrothermal conditions (>410°C), which could have been overlooked based on microthermometric studies of fluid inclusions in quartz only (main growth at 300-320°C). Geochronological constraints on cleft monazite and ZFT, attest that
25   the fluid circulation took place when the host-rock had already cooled below 240-280°C, and heating of the wall-rock lasted for 1-3 My. The impact of the hot fluid circulations on exhumation rates is twofold: (1) by modifying the thermal regime transiently and (2) by resetting the ZFT thermochronometer. Advective heating associated with this hot fluid was spatially restricted to the wall-rock of the Alpine-type cleft, although it may be difficult to evaluate the impact of possible pervasive fluid circulation during the faulting of the granite host-rock. A circulating fluid exceeding the cleft host rock temperature by
30   150-250°C implies very dynamic pathways to efficiently drain fluids over large distance at mid-crustal levels, with a local impact once it migrates through the cleft. Further constraints on the permeability and fluid flux required for this advective heating by hot fluids would require modelling, extensive field mapping of the geological structures (geometry of the vein

network and its possible channelization) and geochemical and petrological studies to characterize reactions and mass transfer associated with the fluid circulation.

Author contribution

EJ was the principal investigator of this collaborative project. Most measurements were done by AG'H during his PhD
5   project co-supervised with A-MS-G. Mineral separation, petrography of fluid inclusions and microthermometric measurement were done in collaboration with DG, the LA-ICP-MS measurements on fluid inclusions with MCB. The ZFT analyses were supervised by MB. Sample were collected on the field with EG and RDAG. The timing and conditions of deformation, metamorphism, and fluid circulations in the ECM were thoroughly discussed and controlled with MR.

References

10   Austrheim, H. and Griffin, W.: Shear Deformation and Eclogite Formation Within Granulite-Facies Anorthosites of the Bergen Arcs, Western Norway. Chem. Geol. 50, 267–281. https://doi.org/10.1016/0009-2541(85)90124-X, 1985.

Bellanger, M., Augier, R., Bellahsen, N., Jolivet, L., Monié, P., Baudin, T. and Beyssac, O.: Shortening of the European Dauphinois margin (Oisans Massif, Western Alps): New insights from RSCM maximum temperature estimates and 40Ar/39Ar in situ dating. J. Geodyn. 83, 37–64. https://doi.org/10.1016/j.jog.2014.09.004, 2015.

15   Bergemann, C., Gnos, E., Berger, A., Whitehouse, M., Mullis, J., Wehrens, P., Pettke, T. and Janots, E.: Th-Pb ion probe dating of zoned hydrothermal monazite and its implications for repeated shear zone activity: An example from the Central Alps, Switzerland. Tectonics 36, 2016TC004407. https://doi.org/10.1002/2016TC004407, 2017.

Berger, A., Gnos, E., Janots, E., Whitehouse, M., Soom, M., Frei, R., Waight, T.E.: Dating brittle tectonic movements with cleft   monazite: Fluid-rock   interaction   and   formation   of   REE   minerals.   Tectonics   32,   1176–1189.
20   https://doi.org/10.1002/tect.20071, 2013.

Bodnar, R.J.: Interpretation of Data from Aqueous-Electrolyte Fluid Inclusion. In:(Samson, I., Alderton, A., and Marshall, D. Eds.), *Fluid Inclusions : Analysis and Interpretation*. Mineralogical Association of Canada, 2003.

Boutoux, A., Verlaguet, A., Bellahsen, N., Lacombe, O., Villemant, B., Caron, B., Martin, E., Assayag, N. and Cartigny, P.: Fluid systems above basement shear zones during inversion of pre-orogenic sedimentary basins (External Crystalline
25   Massifs, Western Alps). Lithos 206–207, 435–453. https://doi.org/10.1016/j.lithos.2014.07.005, 2014.

Boutoux, A., Bellahsen, N., Nanni, U., Pik, R., Verlaguet, A., Rolland, Y. and Lacombe, O.: Thermal and structural evolution of the external Western Alps: Insights from (U–Th–Sm)/He thermochronology and RSCM thermometry in the Aiguilles Rouges/Mont Blanc massifs. Tectonophysics 683, 109–123. https://doi.org/10.1016/j.tecto.2016.06.010, 2016.

Can, I.: A new improved Na/K geothermometer by artificial neural networks. Geothermics 31, 751–760.
30   https://doi.org/10.1016/S0375-6505(02)00044-5, 2002.

Cenki-Tok, B., Oliot, E., Rubatto, D., Berger, A., Engi, M., Janots, E., Thomsen, T.B., Manzotti, P., Regis, D., Spandler, C., Robyr, M. and Goncalves, P.: Preservation of Permian allanite within an Alpine eclogite facies shear zone at Mt Mucrone, Italy: Mechanical and chemical behavior of allanite during mylonitization. Lithos 125, 40–50. https://doi.org/10.1016/j.lithos.2011.01.005, 2011.

Debon, F., Guerrot, C., Menot, R.P., Vivier, G. and Cocherie, A.: Late Variscan granites of the Belledonne massif (French
western Alps): an early Visean magnesian plutonism. Schweiz. Mineral. Petrogr. Mitteilungen 78, 67–85, 1998.

Derry, L.A., Evans, M.J., Darling, R. and France-Lanord, C.: Hydrothermal heat flow near the Main Central Thrust, central
Nepal Himalaya. Earth Planet. Sci. Lett. 286, 101–109. https://doi.org/10.1016/j.epsl.2009.06.036, 2009.

5   Diamond, L.-W. and Tarantola, A.: Interpretation of fluid inclusions in quartz deformed by weak ductile shearing:
Reconstruction of differential stress magnitudes and pre-deformation fluid propoerties. Earth Planet. Sci. Lett. 417, 107–
119. https://doi.org/10.1016/j.epsl.2015.02.019, 2015.

Dumont, T., Champagnac, J.-D., Crouzet, C. and Rochat, P.: Multistage shortening in the Dauphiné zone (French Alps): the
record of Alpine collision and implications for pre-Alpine restoration. Swiss J. Geosci. 101, 89–110.
10   https://doi.org/10.1007/s00015-008-1280-2, 2008.

Engi, M., Lanari, P. and Kohn, M.J.: Significant Ages—An Introduction to Petrochronology. Rev. Mineral. Geochem. 83, 1–
12. https://doi.org/10.2138/rmg.2017.83.1, 2017.

Fabre, C., Boiron, M.-C., Dubessy, J., Cathelineau, M. and Banks, D.A.: Palaeofluid chemistry of a single fluid event: a bulk
and in-situ multi-technique analysis (LIBS, Raman Spectroscopy) of an Alpine fluid (Mont-Blanc). Chem. Geol. 182,
15   249–264. https://doi.org/10.1016/S0009-2541(01)00293-5, 2002.

Fügenschuh, B. and Schmid, S.M. Late stages of deformation and exhumation of an orogen constrained by fission-track data:
A case study in the Western Alps. GSA Bull. 115, 1425–1440. https://doi.org/10.1130/B25092.1, 2003.

Gasquet, D., Bertrand, J.-M., Paquette, J.-L., Lehmann, J., Ratzov, G., Guedes, R.D.A., Tiepolo, M., Boullier, A.-M.,
Scaillet, S. and Nomade, S.: Miocene to Messinian deformation and hydrothermal activity in a pre-Alpine basement
20   massif of the French western Alps: new U-Th-Pb and argon ages from the Lauziere massif. Bull. Soc. Geol. Fr. 181,
227–241. https://doi.org/10.2113/gssgfbull.181.3.227, 2010.

Glotzbach, C., van der Beek, P.A. and Spiegel, C.: Episodic exhumation and relief growth in the Mont Blanc massif,
Western Alps from numerical modelling of thermochronology data. Earth Planet. Sci. Lett. 304, 417–430.
https://doi.org/10.1016/j.epsl.2011.02.020, 2011.

25   Gnos, E., Janots, E., Berger, A., Whitehouse, M., Walter, F., Pettke, T. and Bergemann, C.: Age of cleft monazites in the
eastern Tauern Window: constraints on crystallization conditions of hydrothermal monazite. Swiss J. Geosci. 108, 55–74.
https://doi.org/10.1007/s00015-015-0178-z, 2015.

Goncalves, P., Oliot, E., Marquer, D. and Connolly, J. a. D.: Role of chemical processes on shear zone formation: an
example from the Grimsel metagranodiorite (Aar massif, Central Alps). J. Metamorph. Geol. 30, 703–722.
30   https://doi.org/10.1111/j.1525-1314.2012.00991.x, 2012.

Grand'Homme, A., Janots, E., Bosse, V., Seydoux-Guillaume, A.M. and Guedes, R.D.A.: Interpretation of U-Th-Pb in-situ
ages of hydrothermal monazite-(Ce) and xenotime-(Y): evidence from a large-scale regional study in clefts from the
western alps. Mineral. Petrol. 1–21. https://doi.org/10.1007/s00710-016-0451-5, 2016.

Hall, D.L., Sterner, S.M. and Bodnar, R.J.: Freezing point depression of NaCl-K-Cl-H$_2$O solutions. Economic Geology 83,

197-202, 1988.

Hofmann, B.A., Helfer, M., Diamond, L.W., Villa, I.M., Frei, R. and Eikenberg, J.: Topography-driven hydrothermal breccia mineralization of Pliocene age at Grimsel Pass, Aar massif, Central Swiss Alps. Schweiz. Mineral. Petrogr. Mitteilungen 84, 271–302, 2004.

5   Janots, E., Berger, A., Gnos, E., Whitehouse, M., Lewin, E. and Pettke, T.: Constraints on fluid evolution during metamorphism from U–Th–Pb systematics in Alpine hydrothermal monazite. Chem. Geol. 326–327, 61–71. https://doi.org/10.1016/j.chemgeo.2012.07.014, 2012.

Leisen, M., Boiron, M.C., Richard, A. and Dubessy, J.: Determination of Cl and Br concentrations in individual fluid inclusions by combining microthermometry and LA-ICPMS analysis: Implication for the origin of salinity in crustal

10   fluids. Chem. Geol. 330-331, 197-206. https://doi.org/10.1016/j.chemgeo.2012.09.003, 2012.

Leloup, P.H., Arnaud, N., Sobel, E.R. and Lacassin, R.: Alpine thermal and structural evolution of the highest external crystalline massif: The Mont Blanc. Tectonics 24, TC4002. https://doi.org/10.1029/2004TC001676, 2005.

Marquer, D. and Burkhard, M.: Fluid circulation, progressive deformation and mass-transfer processes in the upper crust: the example of basement-cover relationships in the External Crystalline Massifs, Switzerland. J. Struct. Geol. , 1992.

15   Moëlo, Y., Palvadeau, P., Meisser, N. and Meerschaut, A.: Structure cristalline d'une ménéghinite naturelle pauvre en cuivre, Cu0,58Pb12,72(Sb7,04Bi0,24)S24. Comptes Rendus Geosci. 334, 529–536. https://doi.org/10.1016/S1631-0713(02)01792-3, 2002.

Mullis, J., Dubessy, J., Poty, B. and O'Neil, J.: Fluid regimes during late stages of a continental collision: Physical, chemical, and stable isotope measurements of fluid inclusions in fissure quartz from a geotraverse through the Central

20   Alps, Switzerland. Geochim. Cosmochim. Acta 58, 2239–2267. https://doi.org/10.1016/0016-7037(94)90008-6, 1994.

Nziengui, J.J.: Excès d'argon radiogénique dans le quartz des fissures tectoniques: implications pour la datation des séries méthamorphiques. L'exemple de la coupe de la Romanche, Alpes Occidentales françaises (Thèse 3ème cycle). Université Joseph Fourier, Grenoble, France, 209 p., 1993.

Oliot, E., Goncalves, P., Schulmann, K., Marquer, D. and Lexa, O.: Mid-crustal shear zone formation in granitic rocks:

25   Constraints from quantitative textural and crystallographic preferred orientations analyses. Tectonophysics 612–613, 63–80. https://doi.org/10.1016/j.tecto.2013.11.032, 2014.

Poty, B.P., Stalder, H.A. and Weisbrod, A.M.: Fluid inclusions studies in quartz from fissures of Western and Central Alps. Schweiz. Mineral. Petrogr. Mitteilungen 717–752, 1974.

Putnis, A. and Austrheim, H.: Fluid-induced processes: metasomatism and metamorphism. Geofluids 10, 254–269.

30   https://doi.org/10.1111/j.1468-8123.2010.00285.x, 2010.

Putnis, A., Jamtveit, B. and Austrheim, H.: Metamorphic Processes and Seismicity: the Bergen Arcs as a Natural Laboratory. J. Petrol. 58, 1871–1898. https://doi.org/10.1093/petrology/egx076, 2017.

Roedder, E. Fluid Inclusions. Mineralogical Society of America, 646 p., 1984.

Rolland, Y., Cox, S., Boullier, A.-M., Pennacchioni, G. and Mancktelow, N.: Rare earth and trace element mobility in mid-

crustal shear zones: insights from the Mont Blanc Massif (Western Alps). Earth Planet. Sci. Lett. 214, 203–219. https://doi.org/10.1016/S0012-821X(03)00372-8, 2003.

Rolland, Y. and Rossi, M.: Two-stage fluid flow and element transfers in shear zones during collision burial-exhumation cycle: Insights from the Mont Blanc Crystalline Massif (Western Alps). J. Geodyn. 101, 88–108. https://doi.org/10.1016/j.jog.2016.03.016, 2016.

Rosenberg, C.L. and Berger, A.: On the causes and modes of exhumation and lateral growth of the Alps. Tectonics 28, TC6001. https://doi.org/10.1029/2008TC002442, 2009.

Rossi, M. and Rolland, Y.: Stable isotope and Ar/Ar evidence of prolonged multiscale fluid flow during exhumation of orogenic crust: Example from the Mont Blanc and Aar Massifs (NW Alps). Tectonics 33, 1681–1709. https://doi.org/10.1002/2013TC003438, 2014.

Rossi, M., Rolland, Y. and Cox, S.F.: Geochemical variations and element transfer during shear-zone development and related episyenites at middle crust depths: insights from the Mont Blanc granite (French-Italian Alps). High-Strain Zones Struct. Phys. Prop. 245, 373–396. https://doi.org/10.1144/GSL.SP.2005.245.01.18, 2005.

Seward, D. and Mancktelow, N.: Neogene Kinematics of the Central and Western Alps - Evidence from Fission-Track Dating. Geology 22, 803–806. https://doi.org/10.1130/0091-7613(1994)022<0803:NKOTCA>2.3.CO;2, 1994.

Shepherd, T.J., Rankin, A.H. and Alderton, D.H.M.: A Practical Guide to Fluid Inclusion Studies. 293pp., 1985.

Sharp, Z.D., Masson, H. and Lucchini, R.: Stable isotope geochemistry and formation mechanisms of quartz veins; extreme paleoaltitudes of the Central Alps in the Neogene. Am. J. Sci. 305, 187–219. https://doi.org/10.2475/ajs.305.3.187, 2005.

Simon-Labric, T., Rolland, Y., Dumont, T., Heymes, T., Authemayou, C., Corsini, M. and Fornari, M.: 40Ar/ 39Ar dating of Penninic Front tectonic displacement (W Alps) during the Lower Oligocene (31–34 Ma). Terra Nova 21, 127–136. https://doi.org/10.1111/j.1365-3121.2009.00865.x, 2009.

Verma, S.P. and Santoyo, E.: New improved equations for NaK, NaLi and SiO2 geothermometers by outlier detection and rejection. J. Volcanol. Geotherm. Res. 79, 9–23. https://doi.org/10.1016/S0377-0273(97)00024-3, 1997.

Whipp, D.M. and Ehlers, T.A. Influence of groundwater flow on thermochronometer-derived exhumation rates in the central Nepalese Himalaya. Geology 35, 851–854. https://doi.org/10.1130/G23788A.1, 2007.

Yamada, R., Tagami, T., Nishimura, S. and Ito, H.: Annealing kinetics of fission tracks in zircon: an experimental study. Chem. Geol. 122, 249–258. https://doi.org/10.1016/0009-2541(95)00006-8, 1995.

Zhang, Y.G. and Frantz, J.D.: Determination of the homogenization temperatures and densities of supercritical fluids in the system NaCl-KCl-CaCl$_2$-H$_2$O using synthetic fluid inclusions. Chem. Geol. 64, 335-350, 1987.

Figures
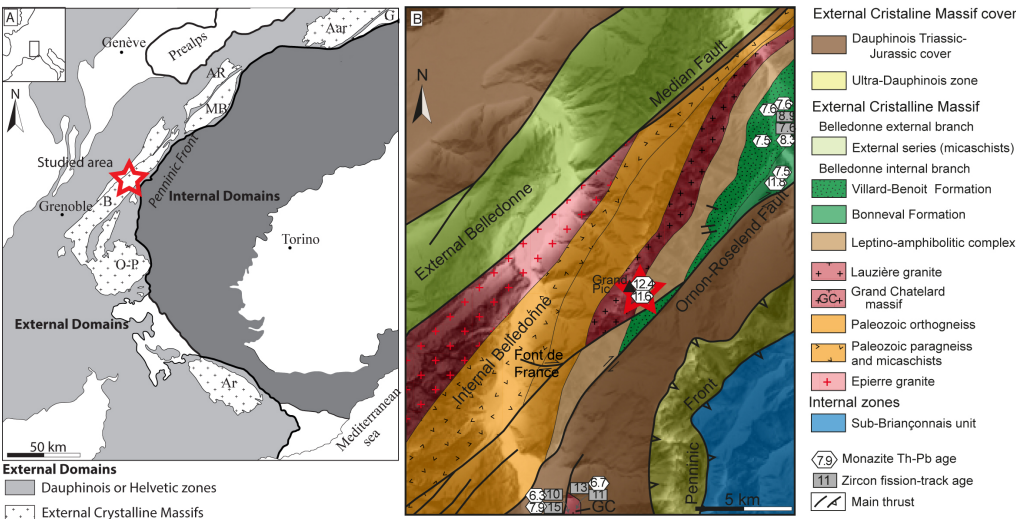
Figure 1: Simplified geological maps showing the location of the investigated area (red star). (A) Western Alps with the location of the External Crystalline Massifs: Aar; G: Gotthard; AR: Aiguilles Rouges; MB: Mont Blanc; B: Belledonne; P: Pelvoux; O: Oisans; Ar: Argentera. (B) Main geological units of the Lauzière massif. Grey rectangles are zircon fission-track central ages (Fügenschuh and Schmid, 2003), white polygons are monazite Th-Pb ages (Gasquet et al., 2010; Grand'Homme et al., 2016).
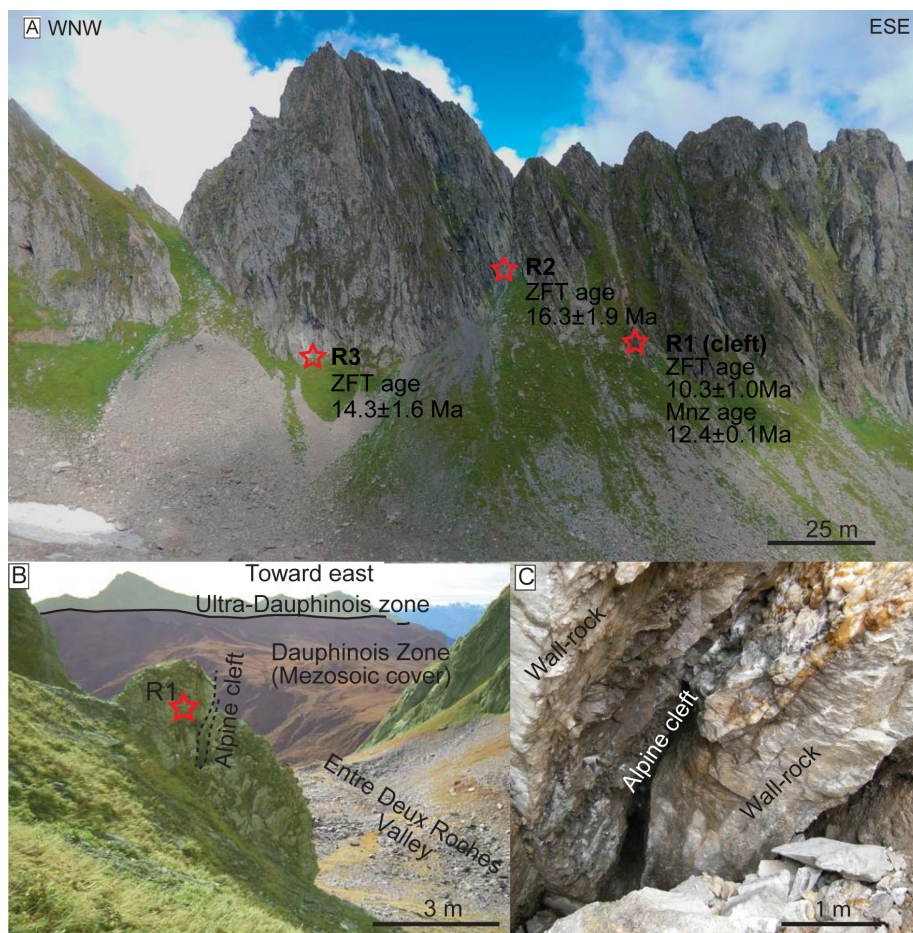
Figure 2: Photographs of the investigated outcrop. (A) *Entre Deux Roches* profile with location and ages of the investigated samples. (B) Alpine-type cleft location with location of the R1 sample taken in the wall-rock of the cleft. The vertical mylonitic shear zones are oriented perpendicular to the vein (C) Detail of the Alpine-type cleft showing the hydrothermal crystals and the leached wall-rock.
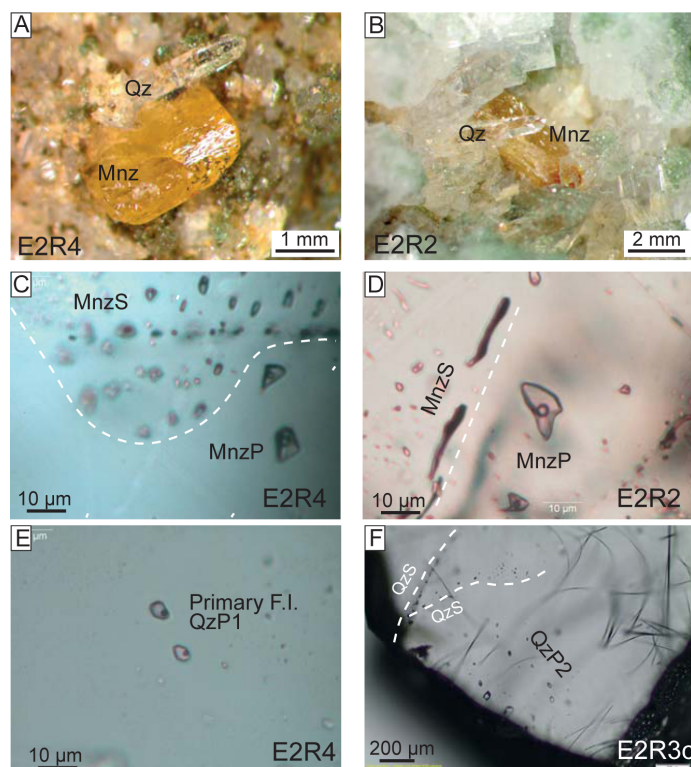
Figure 3: Photographs and microphotographs (C-D-E-F) of cleft quartz (Qz) and monazite (Mnz) crystals and their fluid inclusions. (A) and (B): contiguous quartz and monazite crystals used for fluid inclusion microanalyses (samples E2R4 et E2R2, respectively). (C) and (D): fluid inclusions in monazite: note that primary fluid inclusions (MnzP; around 10 μm) are found in limpid domains whereas secondary fluid inclusions (MnzS; <5 μm) form trails; (E) and (F) Fluid inclusions in quartz: the two populations of primary inclusions (QzP1 and QzP2) have similar morphologies (euhedral with typical size of 10 μm) and are found in limpid quartz domains while the secondary fluid inclusions are smaller and found aligned along trails. Black mineral fibers are meneghinite (Pb$_{13}$CuSb$_7$S$_{24}$; Moëlo et al., 2002)
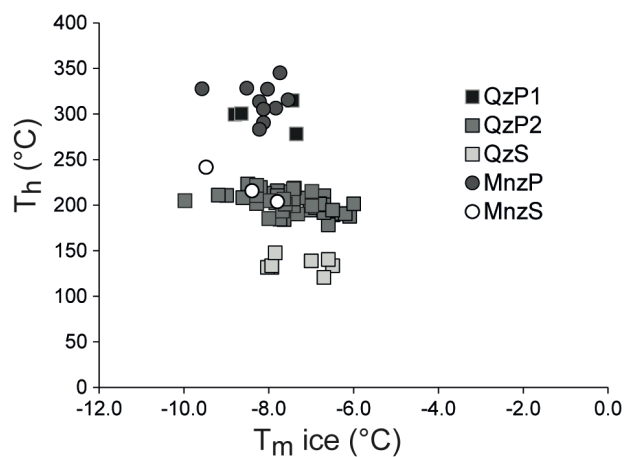
Figure 4: T$_h$ vs. T$_m$ ice diagram of the fluid inclusions data. QzP1: population 1 of primary fluid inclusions in quartz; QzP2: population 2 of primary fluid inclusions in quartz; QzS: secondary fluid inclusions in quartz; MnzP: primary fluid inclusions in monazite; MnzS: secondary fluid inclusions in monazite
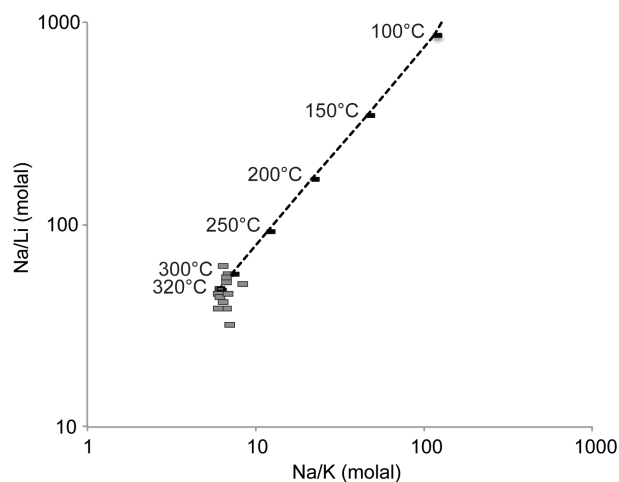
Figure 5: Na/K versus Na/Li ratio measured in quartz fluid inclusions (QzP2). The dash line corresponds to geothermometry calibrations from Verma and Santoyo (1997). The dataset indicates a temperature growth at 300-320°C.
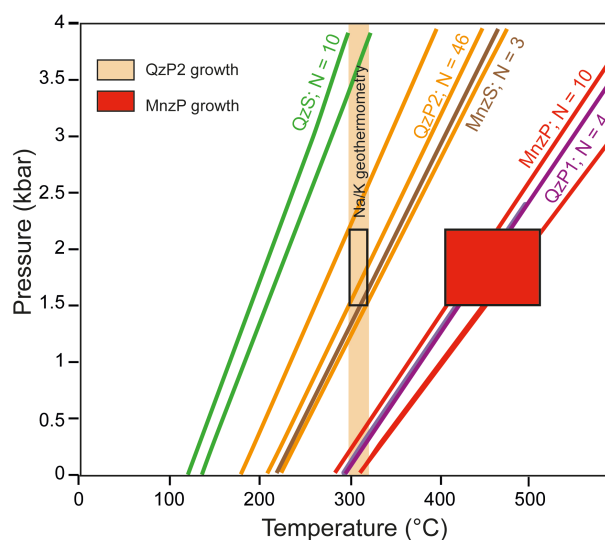
Figure 6: Geothermobarometric results obtained for fluid inclusions of the Alpine-cleft. Mean isochoric P-T relationships calculated from microthermometric measurements of fluid inclusions in monazite and quartz showing three main stages of growth. Fluid inclusion populations and number of analyses are indicated. P-T estimation for the main episode of quartz growth (QzP2) is obtained by the intersection of the T interval determined by the Na/K geothermometer (300-320°C) with the QzP2 isochore. It gives a pressure estimates of 1.5-2.2 kbar for the main phase of quartz growth, that was used to determine the maximal T range (410-520°C) for monazite (MnzP) growth.
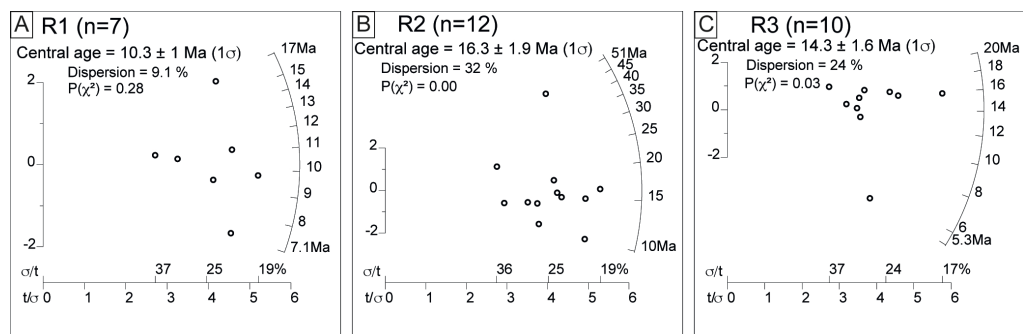
Figure 7: Radial plots of zircon ages in the granite host-rock. (A) *R1* **sample (cleft hanging-wall). (B)** *R2* **sample (~30 m from the**
5   **cleft). (C)** *R3* **sample (~100 m from the cleft)**
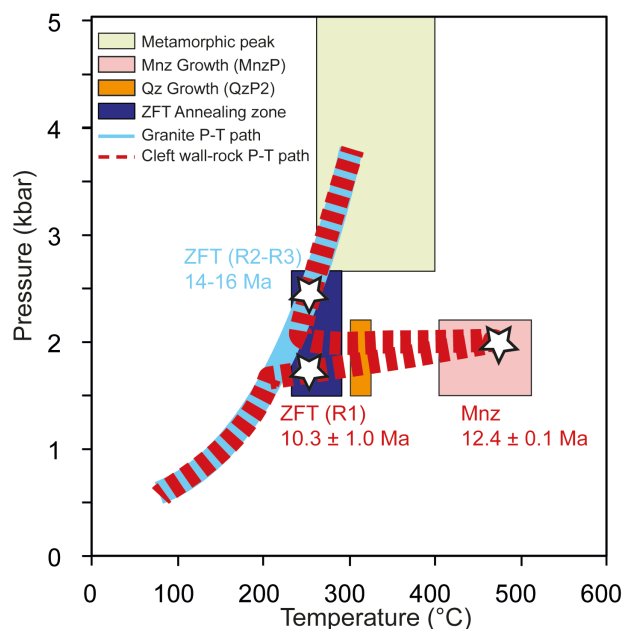
Figure 8: Pressure-temperature (P-T) path for the Lauzière granite host-rock and in the hanging wall of the Alpine-type cleft. Metamorphic peak conditions are not well constrained in the Lauzière massif, and are based on a compilation of metamorphic and geochronological data in the external massifs from the Western Alps (Rolland et al., 2003; Rossi et al., 2005; Simon-Labric et al., 2009; Bellanger et al., 2015). Geochronological constrains provided in this study are represented by stars. The zircon fission track (ZFT) thermochronometer fixes the cooling of the granite (R2-R3) and the cleft (R1) below 240-280°C. Microthermometric and geochronological results on monazite (Mnz) are assumed to represent the onset of hydrothermal activity (red box); while the main hydrothermal growth phase is based on microthermometric study of the fluid inclusions in quartz (QzP2).

Table 1: Microthermometric analyses of fluid inclusions in monazite (Mnz) and quartz (Qz)

Sample	Mineral	Type	T_e (°C)	T_m ice (°C)	T_h (°C)	Population
E2R1	Qz	Primary	-21.3	-7.8	210.4	QzP2
E2R1	Qz	Secondary	-21.3	-6.7	120.6	QzS
E2R1	Qz	Primary	-	-8.2	219.3	QzP2
E2R2	Mnz	Primary	-	-7.5	315.5	MnzP
E2R2	Mnz	Primary	-	-8.0	327.3	MnzP
E2R2	Mnz	Primary	-22.9	-7.7	345.3	MnzP
E2R2	Mnz	Primary	-23.1	-9.6	327.6	MnzP
E2R2	Mnz	Secondary	-	-9.5	241.6	MnzS
E2R2	Mnz	Primary	-22.8	-8.5	328.4	MnzP
E2R2	Qz	Primary	-22.4	-7.6	184.3	QzP2
E2R2	Qz	Primary	-	-7.4	314.9	QzP1
E2R2	Qz	Primary	-	-8.6	208.2	QzP2
E2R2	Qz	Primary	-23.0	-7.7	184.6	QzP2
E2R2	Qz	Primary	-22.7	-7.8	202.8	QzP2
E2R2	Qz	Primary	-	-6.1	187.7	QzP2
E2R2	Qz	Primary	-	-6.5	189.6	QzP2
E2R2	Qz	Primary	-	-6.3	190.8	QzP2
E2R2	Qz	Primary	-	-7.0	194.5	QzP2
E2R2	Qz	Primary	-	-7.4	278.3	QzP1
E2R3a	Mnz	Secondary	-21.2	-8.4	215.7	MnzS
E2R3a	Mnz	Secondary	-	-7.8	203.8	MnzS
E2R3a	Qz	Primary	-	-6.7	200.4	QzP2
E2R3a	Qz	Primary	-	-6.2	190.5	QzP2
E2R3a	Qz	Primary	-21.3	-7.8	215.8	QzP2
E2R3a	Qz	Primary	-	-8.1	212.9	QzP2
E2R3a	Qz	Secondary	-21.3	-6.5	133.5	QzS
E2R3a	Qz	Primary	-	-7.4	218.6	QzP2
E2R3a	Qz	Secondary	-	-6.6	140.4	QzS
E2R3a	Qz	Primary	-	-6.8	201.4	QzP2
E2R3b	Qz	Primary	-21.3	-6.7	200.2	QzP2
E2R3b	Qz	Primary	-21.3	-6.9	197.5	QzP2
E2R3b	Qz	Primary	-	-7.3	207.9	QzP2
E2R3b	Qz	Primary	-21.3	-6.6	178.3	QzP2
E2R3b	Qz	Primary	-22.8	-7.7	214.7	QzP2
E2R3b	Qz	Primary	-	-6.7	210.3	QzP2
E2R3b	Qz	Primary	-	-6.7	191.9	QzP2
E2R3c	Qz	Primary	-21.2	-6.8	201.6	QzP2
E2R3c	Qz	Primary	-	-6.8	201.0	QzP2
E2R3c	Qz	Secondary	-21.2	-7.0	138.9	QzS
E2R3c	Qz	Primary	-21.0	-6.5	194.5	QzP2
E2R3c	Qz	Primary	-	-8.5	223.3	QzP2

E2R3c	Qz	Primary	-	-6.0	201.4	QzP2
E2R4	Mnz	Primary	-	-7.8	306.6	MnzP
E2R4	Mnz	Primary	-	-8.2	313.5	MnzP
E2R4	Mnz	Primary	-	-8.1	305.3	MnzP
E2R4	Mnz	Primary	-	-8.1	290.5	MnzP
E2R4	Mnz	Primary	-	-8.2	283.2	MnzP
E2R4	Qz	Primary	-	-8.8	299.6	QzP1
E2R4	Qz	Primary	-22.8	-9.0	210.7	QzP2
E2R4	Qz	Primary	-	-9.2	211.0	QzP2
E2R4	Qz	Primary	-22.9	-7.5	210.0	QzP2
E2R4	Qz	Primary	-	-7.7	210.3	QzP2
E2R4	Qz	Secondary	-	-7.9	131.6	QzS
E2R4	Qz	Secondary	-	-8.0	131.6	QzS
E2R4	Qz	Secondary	-	-7.9	133.5	QzS
E2R4	Qz	Secondary	-	-7.9	147.7	QzS
E2R31a	Qz	Primary	-	-7.3	213.1	QzP2
E2R31a	Qz	Primary	-	-7.3	199.9	QzP2
E2R31a	Qz	Primary	-	-7.5	202.0	QzP2
E2R31a	Qz	Primary	-	-7.5	193.9	QzP2
E2R31a	Qz	Primary	-	-6.9	203.5	QzP2
E2R31a	Qz	Primary	-	-8.2	217.4	QzP2
E2R31a	Qz	Primary	-	-8.2	200.9	QzP2
E2R31a	Qz	Primary	-	-7.9	186.3	QzP2
E2R31a	Qz	Primary	-	-7.2	190.9	QzP2
E2R31b	Qz	Primary	-	-9.8	201.1	QzP2
E2R31b	Qz	Primary	-	-7.9	200.9	QzP2
E2R31b	Qz	Primary	-	-6.9	199.2	QzP2
E2R31b	Qz	Primary	-	-7.0	200.4	QzP2
E2R31b	Qz	Primary	-	-6.9	211.0	QzP2

Table 2: Compositional data of fluid inclusions (QzP2) obtained from LA-ICPMS measurements. Temperatures (T) were estimated using the Na/K geothermometers of Can (2002)

Sample	Element concentrations (ppm)				T (°C)
	Li (7)	Na (23)	K (39)	Sr (88)	
DL	*26*	*1836*	*180*	*1*	
E2R3A	210	43300	11800	430	320
E2R3A	340	43300	11400	530	310
E2R3B	250	43300	11300	470	310
ER31A	290	43300	12000	350	320
ER31A	290	43300	12700	690	330
ER31A	230	43300	11200	370	310
ER31A	320	43300	12000	1440	320
ER31A	410	43300	10900	1050	310
ER31A	300	43300	12500	1090	320
E2R31B	290	43300	11200	740	310
E2R31B	240	43300	11500	770	310
E2R31B	270	43300	12400	850	320
E2R31B	340	43300	12800	1080	330
E2R31B	260	43300	9200	690	280

DL: detection limit